Electronic Spectroscopy of Gemcitabine and Derivatives for Possible Dual-Action Photodynamic Therapy Applications

Abdelazim M. A. Abdelgawwad,[a] Daniel Roca-Sanjuán,[a] and Antonio Francés-Monerris[a,*]

a) Institut de Ciència Molecular, Universitat de València, 46071 València, Spain

*A.F.-M. e-mail: antonio.frances@uv.es

ABSTRACT

In this study we explore the molecular basis of combining photodynamic therapy (PDT), a light-triggered targeted anticancer therapy, with the traditional chemotherapeutic properties of the well-known cytotoxic agent gemcitabine. A photosensitizer prerequisite is significant absorption of biocompatible light in the visible/near IR range, ideally between 600 and 1000 nm. We use highly accurate multiconfigurational CASSCF/MS-CASPT2/MM and TD-DFT methodologies to determine the absorption properties of a series of gemcitabine derivatives with the goal of red-shifting the UV absorption band toward the visible region and facilitating triplet state population. The choice of the substitutions and thus the rational design is based on important biochemical criteria and on derivatives whose synthesis is reported in the literature. The modifications tackled in this work consist of: i) substitution of the oxygen atom at O2 position with heavier atoms (O→S and O→Se) to red-shift the absorption band and increase the spin-orbit coupling, ii) addition of a lipophilic chain at the N7 position to enhance transport into cancer cells and slow down gemcitabine metabolism, and iii) attachment of aromatic systems at C5 position to further enhance redshift. Results indicate that the combination of these three chemical modifications markedly shifts the absorption spectrum towards the 500 nm region and beyond and drastically increases spin-orbit coupling values, two key PDT requirements. The obtained theoretical predictions encourage biological studies to further develop this anticancer approach.
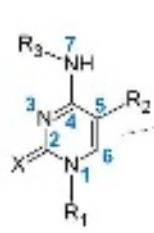
I. INTRODUCTION

Cancer is a multifaceted and devastating disease characterized by the unregulated proliferation of aberrant cells. Traditional chemotherapy, a prevalent treatment approach, relies on the use of cytotoxic drugs or prodrugs that halt cell cycle through a variety of mechanisms.[1,2] Among these modes of action, DNA functioning is a common therapeutic target due to its fundamental role in cells. Classical examples are the DNA alkylation exerted by platinum-based drugs[3] or the action of nucleoside analogues[4] that are incorporated into DNA stopping the DNA polymerase activity. Cladribine, cytarabine, gemcitabine, and others are well-known examples of nucleoside analogues widely used in clinical oncology.[5,6] Whereas the cytotoxicity of these drugs is potent, and these treatments can be very effective as anticancer agents as demonstrated by clinical experience, they are usually associated to severe side effects due to poor specificities toward cancerous cells.[7]

In this context, the development of the so-called targeted therapies aims at decreasing systemic effects by adding spatiotemporal control of the biological damage. One successful and promising possibility is represented by light-triggered therapies, which use light to activate a photosensitizer (PS) innocuous in the dark although highly toxic upon light exposure, *i.e.,* the excitation energy is transformed into the actual biological damage.[8,9] Classical photodynamic therapy (PDT) is one of the most used approaches, which relies on the photoproduction of highly oxidant species through the reaction between the activated PS and O_2 present in the solid tumor. PDT mechanisms also include acute inflammation caused by immune response stimulation and vascular shutdown leading to tumor infarction.[10] This work aims to combine the inherent cytotoxic behavior of a nucleoside analogue with selective O_2 photoactivation by tuning the chemical structure of the original anticancer agent gemcitabine **4** (Chart 1). The fine tuning is guided by chemical modifications described in the literature, in combination with *ab initio* multiconfigurational quantum-chemistry calculations used to describe in detail the molecular absorption properties.
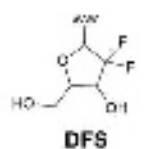
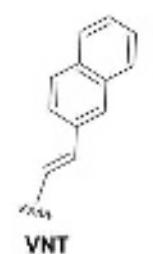| Structure	X	R₁	R₂	R₃
1	O	H	H	H
2	S	H	H	H
3	Se	H	H	H
4	O	DFS	H	H
4a	O	DFS	H	SQ
4b	O	DFS	H	COCH₃
4c	O	DFS	VNT	H
4d	O	DFS	TFS	H
4e	O	DFS	TFS	COCH₃
5	S	DFS	H	H
5a	S	DFS	H	SQ
5b	S	DFS	H	COCH3
5c	S	DFS	VNT	H
5d	S	DFS	TFS	H
6	Se	DFS	H	H
6a	Se	DFS	H	SQ
6b	Se	DFS	H	COCH3
6c	Se	DFS	VNT	H
6d	Se	DFS	VNT	COCH3
6e	Se	DFS	TFS	H
6f	Se	DFS	TFS	COCH3
6g	Se	DFS	TTFS	H
6h	Se	DFS	TTFS	COCH3

X: Heavy atom substitution
R₁: Cytotoxic effects
R₂: Enhanced optical properties
R₃: Transport and self-assembly properties.

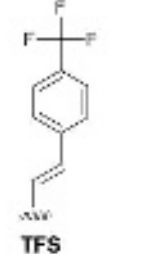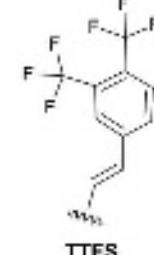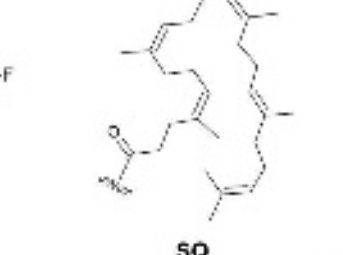Chart 1. Structure of gemcitabine **4** and proposed modifications in this work.

Gemcitabine (**4**) is a cytosine (**1**) derivative (Chart 1) with demonstrated efficacy against a wide range of solid tumors such as pancreatic, non-small lung, breast, and ovarian cancers.[11–13] **4** is a prodrug that is phosphorylated in the intracellular medium to gemcitabine diphosphate and gemcitabine triphosphate, the active forms,[14] thus acting as an analogue of the natural nucleoside cytidine. On the one hand, gemcitabine diphosphate inhibits ribonucleotide reductase, an enzyme that catalyzes the generation of deoxynucleoside triphosphates necessary for DNA synthesis.[14] On the other hand, the activated drug gemcitabine triphosphate incorporates at the end of the elongating DNA strand. After the addition of one more deoxynucleotide, the DNA polymerases are unable to proceed since **4** at the penultimate position prevents the action of DNA repair mechanisms.[15] However, it is worth noting that gemcitabine is prone to rapid deamination in the bloodstream, resulting in the formation of an inactive metabolite known as 2',2'-difluorodeoxyuridine.[15] These pharmacokinetic characteristics contribute to the relatively short half-life of gemcitabine and necessitate high dosing strategies to maintain therapeutic efficacy. Therefore, different modifications on **4**, especially at N7 position (R₃) (Chart 1), have been developed to improve its metabolic stability and cytotoxic activity without affecting its mode of action.[15] One of these modifications involves the chemical covalent linkage of squalene (**SQ**, Chart 1), a well-known intermediate in the cholesterol biosynthesis pathway.[16] Couvreur and co-workers proved that this **SQ**-gemcitabine association **4a** self-assembles and form nanoparticles enhancing the anticancer efficacy as compared to standalone **4** in solution.[16,17] In light of these attractive properties offered by the **SQ** moiety, we have incorporated this modification in the rational design of a suitable PS based on **4** reported in this work.

DNA absorbs light in the UVB and, to a lesser extent, UVA regions of the electromagnetic spectrum.[18,19] Photostability is a fundamental characteristic of DNA[18,20,21] emerging from the outstanding ability of individual nucleobases to dissipate the electronic excitation energy through non-adiabatic processes mediated by readily accessible crossings between excited and ground state potential energy surfaces,[22,23] although the multichromophoric nature[19,20,24] of nucleic acids opens secondary routes that generate well-known photodamage that needs to be properly repaired by the nucleotide excision repair pathway.[25] The most important bright state of DNA nucleobases, nucleosides, and nucleotides is of $^1(\pi,\pi^*)$ nature, whose evolution dictates the intrinsic ultrafast dynamics that imply extremely short excited-state lifetimes at the sub-picosecond scale. Overall, that the triplet population quantum yield of canonical DNA nucleobases[26] is very small although detectable.[27]

Taking the fundamental properties of the DNA canonical nucleobases into consideration, and the strong similarities between **4** and the canonical DNA nucleobase **1** in terms of optical properties, the chemical modification of **4** to red shift the absorption far from the UV region is of utmost importance. The goal is to avoid harmful DNA absorption and maximize the light biocompatibility and penetration capacities into solid tissues by targeting the so-called therapeutic window between 600-1000 nm, *i.e.,* the red/near IR region. On the other hand, PDT mechanisms constitute bimolecular photosensitization processes that require sufficiently long-lived and thus reactive excited electronic states, therefore, this feature is also desirable in a potential PS.[28,29] In this regard, the bioisosteric substitution of the carbonyl oxygen atom at position 2 (X=O) by heavier atoms (X=S and Se, Chart 1) contributes to both requirements, *i.e.,* the red-shift of the absorption properties and the excited-state lifetime extension through the population of triplet excited states by increasing intersystem crossing rates. These substitutions have been systematically studied in this work. Moreover, as shall be demonstrated below, further red shift of the spectrum is achieved by appending aromatic systems of moderate sizes at position 5. The choice of the substituents is based on derivatives whose synthesis is reported in the literature.

In this contribution we employ the multiconfigurational complete-active-space self-consistent-field (CASSCF), the multireference complete active space second-order perturbation theory (CASPT2) methods,[30–33][30,34], well established as reference methods to describe the excited electronic states of organic systems[34,35], including nucleobases[36–41], to predict the light absorption properties of each structure depicted in Chart 1. Spectra in water solution are computed in water boxes simulated with classical molecular dynamics (MD) and hybrid quantum mechanics/molecular mechanics (QM/MM) methods. Our findings indicate that the structures **6g** and **6h** exhibit the most red-shifted absorption spectra and the largest singlet-triplet spin-orbit coupling (SOC) values. These effects are produced by the combination of a O→Se replacement and the presence of a trifluoronated styrene derivative **TTFS** at the C5 position. These results constitute an *in-silico* rational design of PS that could point to a novel dual anticancer action by combining both classical chemotherapeutic and PDT approaches.

II. COMPUTATIONAL DETAILS

a) Geometry optimizations

All ground-state geometries presented in Chart 1 have been optimized using density functional theory, in particular, employing the popular hybrid B3LYP functional in combination with the 6-31G* basis set[42] as implemented in the Gaussian 16 software[43]. No symmetry restrains were imposed. This level of theory was successfully employed in previous spectroscopic studies related to DNA nucleobases[27,37,44–46]. Solvent effects (water) were included through the polarizable continuum model (PCM) method as implemented in the Gaussian 16 software, using the default settings. Frequency calculations were performed on all geometries to ensure the absence of any negative eigenvalue in the Hessian matrix. The time-dependent DFT (TD-DFT/B3LYP) method with the 6-31G* basis set was also used to optimize the triplet state of structure **6h** in water solution, using as well the PCM Gaussian 16 default settings. The nature of the lowest-lying triplet state at the TD-DFT level was ensured by comparison with the CASSCF triplet wave function.

b) Multiconfigurational computations *in vacuo*

The state-average (SA)-CASSCF[47,48] method in combination with the double-ζ relativistic correlation-consistent atomic natural orbitals (ANO-RCC-VDZP) basis set[49] was used to build multiconfigurational wave functions on top of the DFT/B3LYP/6-31G* optimized geometries.[49] Several active spaces were considered and validated in the Supplementary Information (Table S1). An active space of 14 electrons distributed into 10 molecular orbitals [hereafter, CAS(14,10)] was used for compounds with R_2 = H (see Chart 1), whereas a CAS(14,12) is used for systems with R_2 = **VNT**, **TFS**, or **TTFS**. Figures S1-S20 display the SA-CASSCF natural orbitals employed in this work. The ANO-RCC-VDZP basis set was validated by comparing the excitation energies calculated with this basis set with those obtained with the triple-ζ ANO-RCC-VTZP basis set for structures **1**, **2** and **3** (Table S2). The impact of the number of roots (6, 9, and 12) in the SA procedure of the CASSCF method on the excitation energies is also assessed (Table S3). The small deviations found allow to conclude that 6 states can be safely used to compute the absorptions of the oxygen-containing chromophores, whereas 9 states are computed in the SA-CASSCF procedure in the case of compounds containing S and Se. These settings apply to all *in vacuo* and QM/MM multiconfigurational calculations.

The necessary electron dynamic correlation was calculated with both the state-specific (SS) and multi-state (MS)-CASPT2 methods on top of the SA-CASSCF wave functions. The SS-CASPT2 method has been employed for validation purposes, whereas both SS- and MS-CASPT2 methods are used to compute the trends in the absorption properties (compare Figure 1 below with Figure S21). The MS-CASPT2 method is used to compute the absorption spectra in water since it provides absorption energies closer to the experimental records likely due to a better de-mixing of the various bright and dark states, as previously reported in the literature for small aromatic systems.[33,50] An imaginary level-shift of 0.2 a.u. was used in order to minimize the effect of weakly-interacting intruder states. The ionization potential electron affinity (IPEA) shift[51] was set to the recommended value of 0.0 a.u., according to previous studies on related systems.[36–38,52]

Scalar relativistic effects were described in all multiconfigurational calculations with the second-order Douglas-Kroll and Hess (DKH2) Hamiltonian. The validity of this description was assessed on selenocytosine (**3**) by contrasting the results with those obtained with the third-order DKH3 Hamiltonian[53] (see Table S4). Results indicate that both methods provide extremely similar results, with only slight differences appreciated for the oscillator strength values, without any effect on the spectral properties. Consequently, scalar relativistic effects are described at the DKH2 level throughout this work.

Oscillator strengths (*f*) were computed using the following equation as described in a previous work[54]:

$$f = \frac{2}{3} \Delta E \ (TDM)^2$$

where ΔE represents the CASPT2 vertical excitation energy, and TDM corresponds to the transition dipole moment between the initial φ_1 and final φ_2 electronic states in the SA-CASSCF method computed in the dipole gauge. TDM is calculated as $TDM = \langle \varphi_1 | \hat{\mu} | \varphi_2 \rangle$, where $\hat{\mu}$ refers to the dipole moment operator.

SOC matrix elements $\langle T_{x,m_s=-1,0,1} | \hat{H}_{SO} | S_y \rangle$ were computed using the CASSCF wave functions, mixing the first 9 singlets and 9 triplet states, thus resulting in a total of 36 spin-orbit (SO) states except for compounds **1** and **2**, for which 6 singlet and 6 triplet states were considered. The SOC complex vector norms $|\hat{H}_{SO}(T_{x,m_s=-1,0,1}/S_y)|$ were obtained as the square root of the sum of the absolute square of each m_s component of the triplet state T_x with the corresponding singlet state S_y. The effective one-electron spin–orbit Hamiltonian was derived from atomic mean field integrals, employing the RASSI method[55,56] as implemented in OpenMolcas. These calculations were specifically performed for structures **1**, **2**, **3**, **4**, **5**, **6**, and **6h** to assess the heavy atom effect.

All SS- and MS-CASPT2 calculations were performed with the OpenMolcas software package without imposing any symmetry restrain.[57]

c) Classical molecular dynamics and multiconfigurational QM/MM spectra

Equilibrium classical molecular dynamics (MD) simulations were conducted using the Amber20 package[58] to sample the ground state of molecules **1**, **2**, **3**, **4**, **4b**, **5**, **6**, and **6h** in explicit water solvation. Intra- and intermolecular chromophore parameters were extracted from the generalized Amber force field (GAFF).[59] The restrained electrostatic potential (RESP)[60] procedure was adopted to set the atomic charges at the HF/6-31G* level. Water was simulated with the TIP3P model.[61] Water boxes were built adding solvent molecules around a single solute molecule placed in the center of a truncated octahedral box with a minimum distance between the box edge and the dye of 10 Å. The time step was set to 1 fs. Initially, the system was minimized through 250 steps of the steepest descent algorithm, followed by 250 steps of the conjugated gradient algorithm. Subsequently, the system was progressively heated from 0 to 300 K by means of particle Mesh Ewald dynamics in the NVT ensemble for a total time of 20 ps. A cutoff of 5.0 Å,

the maximum allowed by the system box size, was used throughout all simulations. Production runs were carried out in the NPT ensemble for 100 ns, 100 equally distributed snapshots (80 for **6h**) were extracted from the trajectories for further quantum mechanics/molecular mechanics QM/MM refinement. This consisted in 250 steps of QM/MM ground-state dynamics at the B3LYP/6-31G*/MM level of theory (time step 1 fs), in which the photosensitizer is represented in the QM part and the solvent is treated with MM. The electrostatic embedding was used with a cutoff distance of 5.0 Å for all QM-MM interactions.

Single-point MS-CASPT2 calculations on top of the resulting B3LYP/MM geometries were performed to obtain the UV-Vis multiconfigurational spectra. The set of ΔE and f values for the 100 snapshots (50 for **6h**) were convoluted through Gaussian functions with a full width at half maximum (FWHM) of 0.3 eV centered around each ΔE. For compounds **1**, **2**, **3**, **4**, **4b**, **5**, and **6**, a CAS(14,10) active space was employed. 6 roots were computed for X=O compounds and 9 roots for X=S or Se molecules. For structure **6h**, the spectrum is computed making use of a CAS(14,12) active space. Snapshots with active space instabilities that produced spurious low-energy bands were excluded from the convolution. In all cases the spectrum is generated with more than 85 coordinates (68 for **6h**) The theoretical UV-Vis absorption spectra and cross sections (σ) were computed using the code MULTISPEC developed in our group.[62]

All CASSCF/MS-CASPT2/MM calculations were performed with the OpenMolcas software package[57] and without imposing any symmetry constraint.

d) UV-Vis spectrum for 6h in water with TD-DFT

The UV-Vis spectra for **6h** in water and in the vacuum were computed with the TD-B3LYP/6-311G(d,p) method as implemented in the ORCA 5 program.[63] ΔE and f were computed on top of 70 geometries obtained by using the nuclear ensemble approach (NEA). A Wigner sampling around the ground-state equilibrium geometry was performed using the DFT/B3LYP/6-31G* vibrational normal modes with the Newton-X 2.0 program.[64,65], computing 20 singlet and 20 triplet states. Solvent effects (PCM method) and SOC corrections were included by employing the ORCA 5 default settings.[63] Note that, besides using a different electronic structure method, the PCM method better accounts for the effects of solvent polarizability as compared to the QM/MM scheme described in the previous section. The validation of the non-relativistic description with the 6-311G(d,p) basis set was carried out by performing a comparative analysis at the **6h** ground-state minimum with the zeroth-order regular approximation (ZORA)[66] method in combination with the ZORA-Def2-TZVP basis set for all elements (and Def2-TZVP/C as auxiliary basis set). The SOC operator was treated with RI-SOMF(1). Results are listed in Tables S11 and S12 and show a very small impact of the relativistic effects on the absorption energies and f, thus validating the non-relativistic description with the 6-311G(d,p) basis set.

III. RESULTS AND DISCUSSION

A. Heavy atom effect on the absorption properties of modified nucleobases and nucleotides

This section focuses on the impact of the O→S and O→Se replacements in the absorption properties of the nucleobases **1-3** (R_1 = H) and the nucleosides **4-6** (R_1 = **DFS**). Note that the synthesis of all these compounds is reported in the literature, as summarized in Table 1. Figure 1 and S21 compare the vertical absorption energies (ΔE) and oscillator strengths (f) of the brightest spin-orbit free (SF) $^1(\pi, \pi^*)$ states for all molecules studied in this work (the complete list of singlet states can be found in Tables S5-S7). Neither SOC corrections nor solvent effects are added in Figure 1 and S21; this comparison is then only used to quantify red shifts and screen the molecule with the most interesting optical properties.
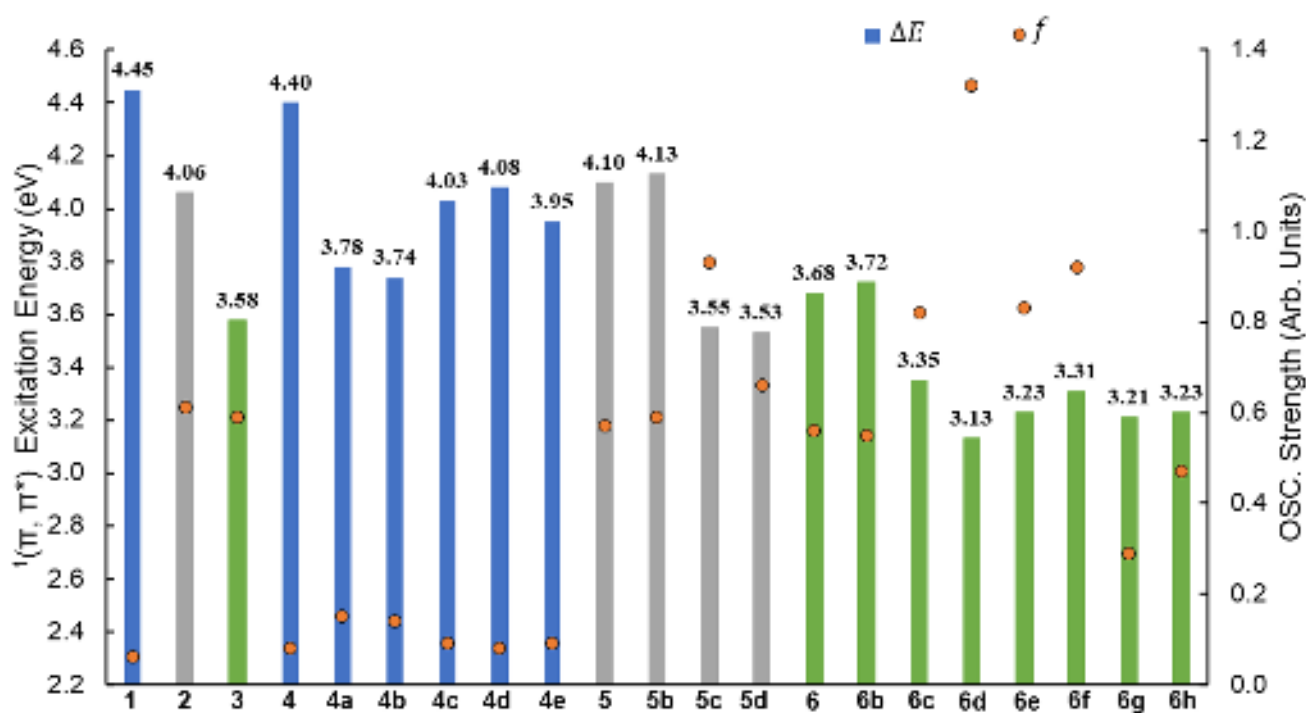

Figure 1. SF MS-CASPT2 excitation energies (ΔEs) and oscillator strengths (f) for each structure depicted in Chart 1. Absorption energies correspond to the first bright $^1(\pi, \pi^*)$ excited state of each molecule computed in vacuum. Tables S5-S7 summarize ΔEs and f for all computed electronic states. Blue, grey and green bars correspond to X = O, S, and Se molecules, respectively.

In the particular case of the **1-3** series, analysis of the ΔE and f values reveals notable differences (Figure 1). The ΔE values for each compound are 4.45 (**1**), 4.06 (**2**), and 3.58 eV (**3**), thus representing a strong red shift from the well-known UVB absorption of cytosine **1** (279 nm) to the UVA zone of 2-selenocytosine **3** (322 nm), and a strong increase of f, which is in turn similar for both **2** and **3**. The absorption properties of **1**[38,45,67] and **2**[28] determined in this work are in reasonable agreement with previous theoretical computations, which employed different basis sets and geometry optimization methods (see

Table 1 for details), and are based on a single geometry (S_0 minimum). On the other hand, to the best of our knowledge, no experimental spectrum of **3** is available yet in the literature, even though its synthesis was reported six decades ago.[68] The SS-CASPT2 method (Figure S21) slightly underestimates the excitation energies of **1-3** with respect to the MS-CASPT2 predictions (Figure 1), although the trends of the absorption energies of the considered compounds are coincident for both methods.

Figure 2 shows the UV-Vis spectrum of **1**, **2**, and **3**, computed with the MS-CASPT2/MM method and including SOC corrections.. Not surprisingly, there is no discernible difference between the spectra provided by SF and SOC-corrected (SO) states due to the low oxygen atomic mass (Figure 2A). The most intense band in structure **1** corresponds to the $^1(\pi o,\pi^*, S_1)$ state with an energy of 4.43 eV (280 nm). On the other hand, the SOC effect is slightly detectable in Figure 2C for structure **3**. The most intense transitions correspond to the population of the $^1(\pi_{se},\pi^*, S_1)$ and $^1(\pi_{se},\pi^*, S_4)$ states, with energies of 2.94 eV (422 nm) and 3.76eV (330 nm), respectively (Figure 2C). The absorption properties of structures **2** are shown in Figure 2B in which the most intense transitions are the $^1(\pi_s,\pi^*, S_1)$ and $^1(\pi_s,\pi^*, S_4)$, with energies of 4.09 eV (303 nm) and 4.68 eV (265 nm), respectively.

The accuracy of the MS-CASPT2 determinations with respect to experimental recordings for X=Se compounds is assessed for the related system 2-Se-Uridine compound in water solution[69] (Table 1 and Figure S23) since, to the best of our knowledge, no experimental records are available for the Se-based systems shown in Chart 1. The maximum absorption band predicted with the MS-CASPT2/MM methodology is 317 nm, close to the experimental value recorded at 307 nm.[69] This analysis gives credit to the QM/MM methodology employed to predict UV-Vis spectra of the Se-based compounds shown in Chart 1.

Table 1. Experimental (λ_{max}^{exp}) and theoretical (λ_{max}^{theo}) maximum band wavelengths (in nm) for the molecules studied in this work. Available experimental literature on the synthesis of the systems characterized in this work is also listed.

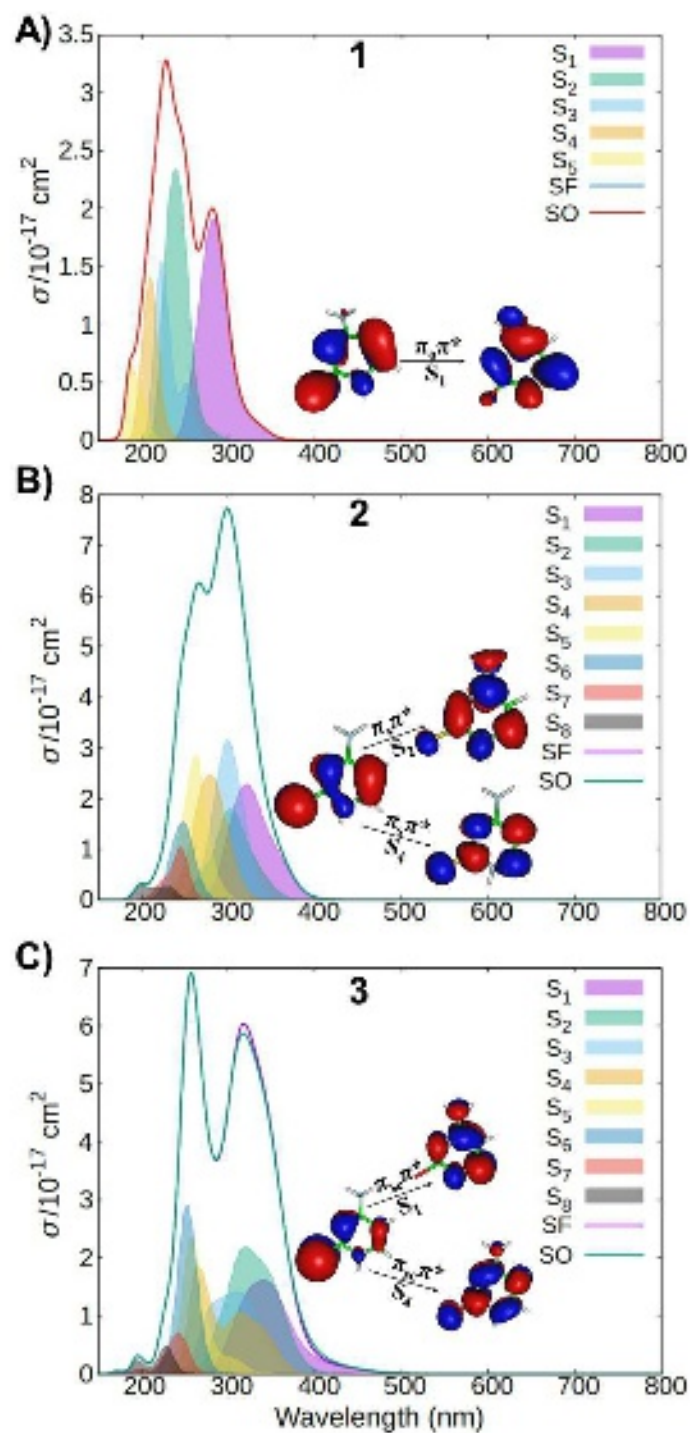| Molecule	$\lambda_{max}^{theo\,a}$ (nm)	λ_{max}^{theo} (nm)	λ_{max}^{exp} (nm)	Synthesis (reference)
1	280	281[b]	264[c]	70
2	303	279[d] 288[e]	269[f]	71,72
3	330	-	-	68,71,73
4	281	254[g]	267[h]	74
5	302	-	-	71,73
6	312	-	-	71,73
4a	327[i]	-	-	16,17
4c	-	-	-	75[j]
4d	-	-	297[k]	76[k]
6g	-	-	-	77[l]
2-Se-Uridine	317[m]	-	307[n]	69

Figure 2. MS-CASPT2/MM cross sections (σ) of structure **1** (A), **2** (B), and **3** (C) based on spin-orbit (SO) and spin-free (SF) electronic states, and contributions from the SF excited states. The CASSCF natural orbitals that characterize the excitation to the most intense bands are also shown. Note the change in the scale of the vertical axis.

Gemcitabine **4** shows an intense absorption band in the experimentally measured spectrum in water peaking at UVC wavelengths (~268 nm, 4.63 eV).[81,82] Previous theoretical calculations based on TDDFT predicted the absorption maximum at 254 nm (4.88 eV, Table 1).[80] This feature strongly resembles that of cytosine **1**, since the only difference between them is the presence of the non-natural difluoro sugar (**DFS**) substituent at the N1 position (R_1), which does not participate directly in the absorption. The absorption spectrum falls within the UV region, thus far from the biological therapeutic window and inappropriate for light-controlled PDT purposes. Similarly, to the **1**-**3** series, the substitution of O by S (**5**) and Se (**6**) also causes an important red shift (from 4.40 to 3.68 eV for **4** and **6**, respectively) and a remarkable increase of the associated f values (Figure 1).

It becomes apparent that the optical properties trends for the **1**-**3** and **4**-**6** series resemble each other. The MS-CASPT2 results predict slight differences in ΔE and f values between these two series, ranging from 0.03 to 0.10 eV (Figure 1). This proves that the effect of the **DFS** component is also very limited in **4**-**6** due to the non-significant participation of the **DFS** moiety in the $^1(\pi,\pi^*)$ transition. Regarding f, structures **6** and **3** exhibit very similar values. The most intense transitions for the former correspond to the population of the $^1(\pi_{se},\pi^*, S_2)$ and $^1(\pi_{se},\pi^*, S_4)$ states, lying at excitation energies (SF states) of 3.05 eV (407 nm) and 3.68 eV (337 nm), respectively (Figure 1).
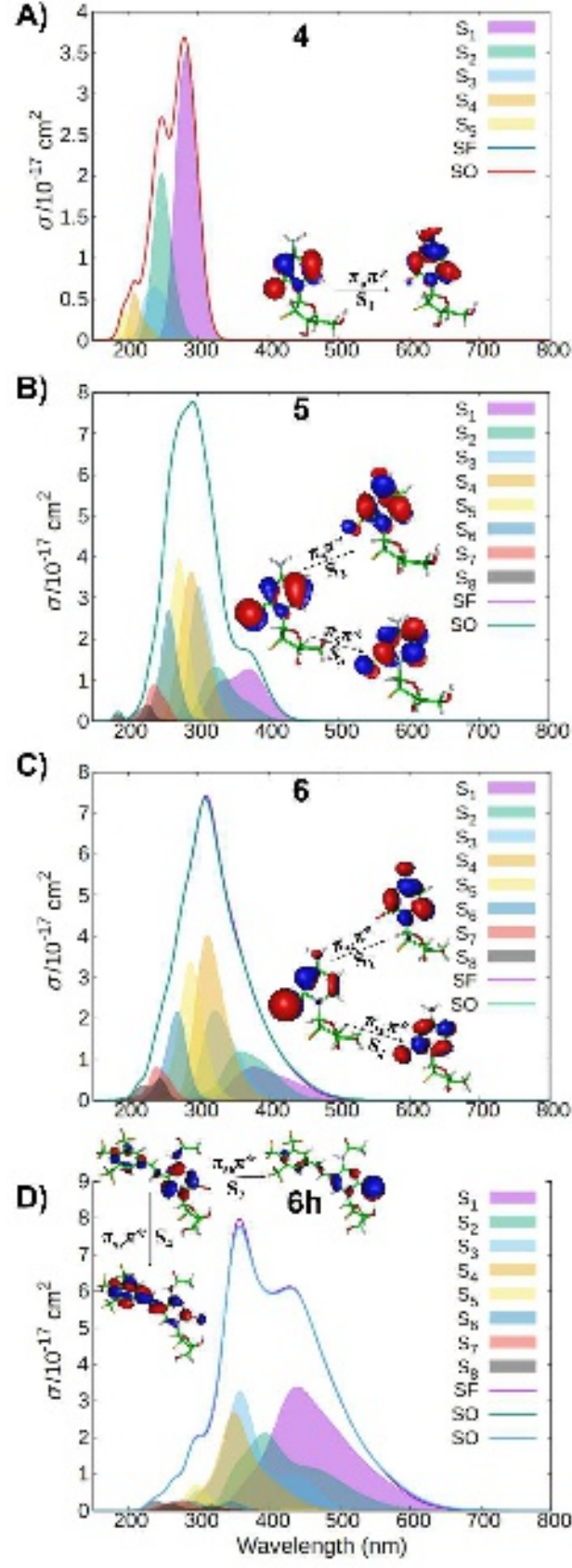
Figure 3. MS-CASPT2/MM cross sections (σ) of structure **4** (A), **5** (B), **6** (C) and **6h** (D) based on spin-orbit (SO) and spin-free (SF) electronic states, and contributions from the SF excited states. The CASSCF natural orbitals that characterize the excitation to the most intense bands are also shown.

Figure 3A-C shows the MS-CASPT2/MM spectra for the series **4-6**, respectively. Notably, it is not surprising that the inclusion of SOC corrections in the simulation of the absorption properties for structures **1**, **2**, **4**, and **5** yields identical results to that of the spectrum based on SF states, since the SOCs induced by oxygen and sulfur are relatively small (Figure 3A and 3B). Contrarily, for structures **3** and **6**, small but observable differences between SF and SO spectra appear, particularly in the second band near 500 nm (Figures 2C and 3C). This spectral deviation is attributed to the presence of Se in these structures.

B. N7 substitution (R$_3$) by the lipophilic squalene substituent

The substitution at the N7 position (R$_3$) of gemcitabine **4** with **SQ** (Chart 1) is a demonstrated strategy to provide self-assembly properties that decrease the rapid metabolism of **4** in the bloodstream.[16,17,83] Consequently, the impact of this substituent on the absorption properties of **4**, **5**, and **6** is carefully assessed in the current work by building the molecular models of the derivatives **4a**, **5a**, and **6a**. The high computational cost associated to the spectra simulation with multiconfigurational quantum-chemistry methods also motivated the study of the systems **4b**, **5b**, and **6b**, which contain the group R$_3$ = -COCH$_3$ as a smaller model representative of the large **SQ** substituent. The ΔE comparison between the set of **SQ** structures (**4a**, **5a**, and **6a**) and the set of corresponding models (**4b**, **5b**, and **6b**) reveal identical values, indicating that the -COCH$_3$ model effectively captures the impact of **SQ** at the N7 position (Figure S21). Consequently, it is reasonable to employ the smaller model for further calculations. The brightest $^1(\pi,\pi^*)$ state of **4b**, **5b** and **6b** (R$_3$ = -COCH$_3$) are very similar with respect to **4**, **5** and **6** (R$_3$ = H) and fall within the error of the method. Therefore, it is reasonable to conclude that the impact of the **SQ** on the absorption properties is very small or negligible.[16] Figure S23 shows the spectrum of **4b** in aqueous environment, which shows that the absorption maximum corresponding to the bright $^1(\pi,\pi^*)$ state peaks at 3.79 eV (327 nm). The synthesis of the gemcitabine derivatives **5a** and **6a** has not been reported yet, however, the strong similarities with **4a** suggest very similar chemical behavior, whereas the heavy atom effect ensures much more adequate photophysical properties for PDT purposes.

C. Extending the π-conjugation by substituting C5 (R$_2$) with aromatic systems

The absorption spectrum of **6** (Figure 3C) is significantly red shifted with respect to the original anticancer agent **4** (Figure 3A). As a matter of fact, in water, the absorption capacities of **6** at wavelengths in the visible region ≥400 nm, which are of interest for biological applications, are superior to that of **4**, which is mainly transparent at these regions. Nevertheless, the absorption capacities of biocompatible light are still limited for **6** and therefore additional substitutions at the C5 position of the cytosine core able to

extend the π-conjugated space deserve a proper characterization. Note that the C5 position of cytosine and, more generally, pyrimidines, is commonly functionalized in nature and some of these derivatives play fundamental biological roles.[39,84,85] For instance, besides a DNA lesion formed upon oxidative damage, 5-formylcytosine is an intermediate in the formation of 5-methylcytosine, which mediates epigenetic regulations of nucleic acids expression.[86] Interestingly, 5-formylcytosine absorbs at longer wavelengths (UVA) as compared to cytosine **1** (mostly UVB), due to the extension of the π-conjugated system. [84,85]

In this work we studied cytidine derivatives with small aromatic systems appended at C5 position (R$_2$) whose synthesis is already described in the literature, considering that the aromatic ring size must have the appropriate size to conjugate both desired optical and biological properties. Thus, it must be sufficiently large to produce a significant red shift towards longer wavelengths, but sufficiently energetic to generate triplet states able to photosensitize oxygen, and reasonably small to retain as much as possible the biological properties of the original gemcitabine **4**. We chose the existing cytidine analogues containing 2-vinylnaphtalene (**VNT**),[75] trifluorostilbene (**TFS**),[76] and tri-trifluorostilbene (**TTFS**)[77] to build the molecular models **4c-4e**, **4d**, **5c**, **5d**, and **6c-6f**. Note that these models differ from the respective synthesized molecules in the fluoride atoms at the sugar moiety, the O→S and O→Se replacements, and/or the appending of **SQ** or -COCH$_3$ at R$_3$.

Figure 1 clearly illustrates the strong red shift induced by the presence of **VNT (4c)** and **TFS (4d)** as compared to the native gemcitabine **4**. In particular, the absorption energy values change from 4.40 to 4.03 and 4.08 eV (308 and 304 nm), respectively. This trend is very similar for structures **5**, **5c**, and **5d**, for which the energies are 4.10, 3.55, and 3.53 eV (302, 349, and 351 nm), respectively. Likewise, for structures **6**, **6c**, and **6e**, the corresponding energy values are 3.68, 3.35, and 3.23 eV (337, 370, and 384 nm), respectively. The reason for these pronounced red shifts is clear and shown in Figure 4. Transitions to the brightest $^1(\pi,\pi^*)$ state involve extended aromatic systems beyond the pyrimidine ring, which is the only chromophore in **4**. Only the most intense transitions for structures **6c** and **6e** are analyzed since these systems show the largest red shifts in vacuum. Analysis of the f values shown also in Figure 1 indicates that structure **6c** exhibits the most intense transition, namely $^1(\pi_{se},\pi^*, S_4)$ state, with a ΔE of 3.35 eV (370 nm) (Figure 4A). On the other hand, the most intense transitions of structure **6e** are the population of $^1(\pi_{se},\pi^*, S_3)$ and $^1(\pi_{se}\pi^*, S_4)$ states with ΔE of 2.96 eV (419 nm) and 3.23 eV (384 nm), respectively (Figure 4B).
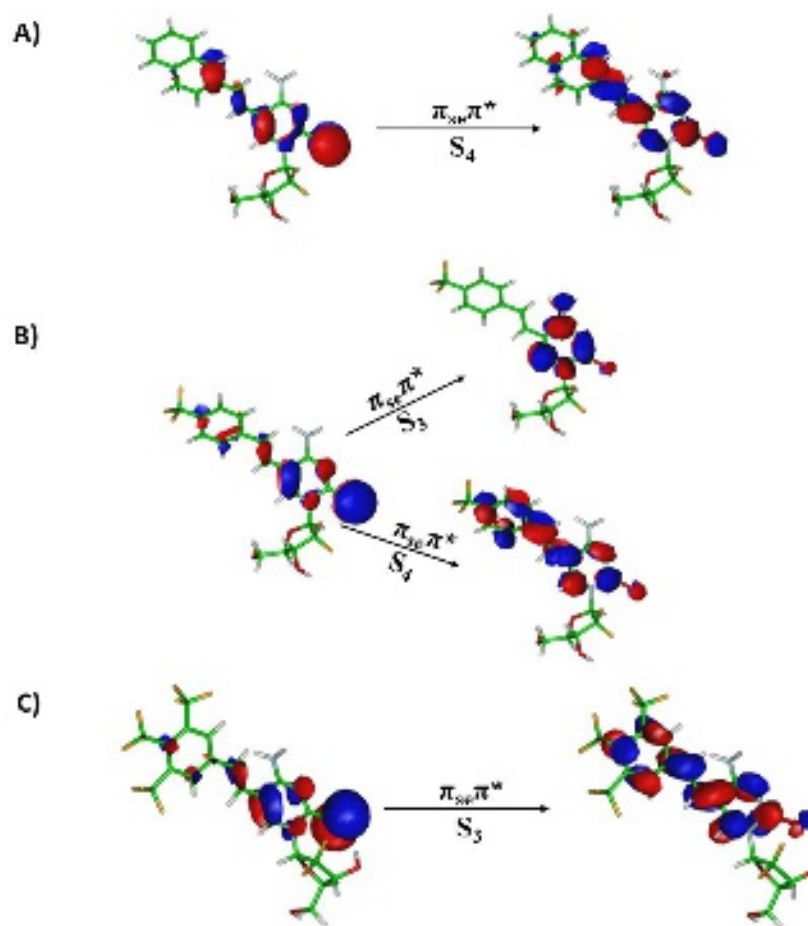
Figure 4. SA-CASSCF natural orbitals for the most intense transition of the lowest lying states for different structures: A) structure **6c**, B) structure **6e** and C) structure **6g**, using the CAS(14,12) active space.

In all series, the structures incorporating the derivative **TFS** possess the lowest excitation energies. The influence of the **SQ** (or the validated -COCH$_3$ truncation) substitution at N7 on the absorption properties of **4d**, **6c** and **6e** can be specifically appraised by comparing their ΔE values with **4e**, **6d** and **6f**, respectively. The presence of -COCH$_3$ results in a slight red shift of 0.13-0.22 eV in case of **4e** and **6d**, while a small blue shift of 0.08 eV occurs in the case of **6f** (Figure 1).

Based on the very good absorption properties offered by the **TFS** group, we also studied the incorporation of additional -CF$_3$ electron-withdrawing groups at the aromatic ring of stilbene, *i.e.,* the **TTFS** fragment (Chart 1). Note that similar nucleobase derivatives have been reported in the experimental literature.[77] Figure 1 shows that the ΔE values calculated for the structures **6g** and **6h** (with and without -COCH$_3$ at R$_3$, respectively) are the lowest of the present work. Compared to **6e** and **6f**, ΔE vary from 3.23 to 3.21 eV (384 to 386 nm) and from 3.31 to 3.23 eV (375 to 384 nm), respectively. The most intense transition for structure **6g** is to the $^1\pi_{se},\pi^*$ (S$_3$) state (Figure 4C), while the brightest states for **6h** are $^1(\pi_{se},\pi^*$, S$_2$) and $^1(\pi_{se},\pi^*$, S$_4$), vertically placed at 2.96 and 3.23 eV (419 and 384 nm), respectively (Figure 1). The absorption spectrum for **6h** in water reveals significant absorption in the 500-600 nm range, and some

absorption exceeding 600 nm (Figure 3D). This absorption is the result of the S_1 and S_2 broad bands, as displayed by the individual contributions to the spectrum shown in Figure 3D.

Overall, the main objective of this study (consisting of decreasing the excitation energy from UV to the visible part of the electromagnetic spectrum) is accomplished, as depicted in Figure 1. The vertical absorption energies clearly decrease from the original DNA nucleobase **1** to the modified DNA nucleotide guided by the rational design of **6h**. The absorption spectrum of **6h** in solution exhibits an extended tail that fully covers the cyan, yellow and orange colors and spans, only partially, the red region (Figure 3D). This feature suggests the potential suitability of structure **6h** for activating the proposed dual chemotherapy/PDT anticancer action in biological conditions, *i.e.,* in water environment.

The correct reproduction of the low-energy tail shape is a challenging task when it comes to simulate spectra with computational methods. The description of this region is as less accurate due to: *i*) the active space control becomes more complicated when computing large number of vertical calculations for an ensemble of coordinates, *ii*) the number of snapshots is limited, and *iii*) the band broadening also depends on the FWHM parameter, which was set to 0.3 eV to obtain the broad band shapes observed in the experiment. Nonetheless, these problems can be mitigated analyzing the results obtained with different nuclear sampling protocols and electronic structure methods.

Figure S24 shows the UV-Vis spectrum computed *in vacuo* and in water by means of the TD-DFT method and the NEA. The spectrum clearly shows intense absorption in the visible region from 400 to 500 nm, while the low energy tail covers wavelengths >500 nm to vanish before 600 nm. The spectrum in solution computed with TDDFT is thus blue shifted with respect to the bands computed with the MS-CASPT2/MM method (Figure 3D). TDDFT however overestimates the absorption energies of these type of molecules with respect to the experimental values, in view of the results provided by Mahar et al. for compound **4** and the current results. Mahar et al. reported a band maximum of 4.88 eV (254 nm)[80] in water while the experimental value is 4.64 eV (267 nm).[81] Similarly, the B3LYP/MM spectrum computed in the present work for compound **2** places the first band maximum at 5.06 eV (245 nm), as displayed in Figure S25, while the experimental value is recorded at 4.61 eV (269 nm, see Table 1). It is therefore reasonable to consider Figures 3D and S24 as upper and lower boundaries, respectively, thereby ensuring the absorption of **6h** in the green (520-565 nm) and yellow (565-590 nm) regions with a tail likely exceeding 600 nm. **6h** thus represents an attractive prototype for light-triggered therapies, whereas species **6d** and **6f** should be considered as equally interesting in terms of absorption properties.

D. Triplet states population and O₂ photosensitization capacities

The primary aim of this study is to propose a modification that could potentially enable PDT processes. In order to quantify the heavy atom effect in the photo-induced intersystem crossing dynamics and triplet population, the singlet-triplet SOC[87] values were computed at the Franck-Condon geometries of **1, 2, 3, 4, 5, 6**, and **6h**. As demonstrated in Table 2, much larger SOCs are predicted for structures **3** and **6** as compared to the analogue structures with the much lighter oxygen atom. The large SOCs between singlet

and triplet states (Table 2), which are typical of molecular systems bearing Se atom,[88,89] strongly support the population of triplet states as a dominant excited-state relaxation pathway.

Table 2. SOC complex vector norms (see Computational Details) in cm^{-1} for structures **1, 2, 3, 4, 5**, **6** and **6h**. Data obtained with the CASSCF(14,10) method in vacuum. Note that T_x encompasses the three m_s components of the triplet state.

$\left\|\hat{H}_{SO}(T_x/S_x)\right\|$	1	2	3	4	5	6	6h
$T_1 - S_0$	0	0	0	1	23	187	9
$T_2 - S_0$	0	0	0	1	88	376	305
$T_3 - S_0$	0	78	359	36	4	7	629
$T_4 - S_0$	23	47	232	20	46	217	41
$T_1 - S_1$	0	0	0	8	121	556	621
$T_2 - S_1$	0	0	0	10	38	317	454
$T_3 - S_1$	0	85	433	27	34	85	211
$T_4 - S_1$	14	82	377	34	4	16	18
$T_1 - S_2$	26	117	590	26	29	237	147
$T_2 - S_2$	19	38	75	18	82	242	306
$T_3 - S_2$	22	0	1	11	10	39	186
$T_4 - S_2$	6	0	0	6	88	418	264
$T_1 - S_3$	28	37	63	26	30	78	199
$T_2 - S_3$	19	139	715	16	3	1	140
$T_3 - S_3$	7	0	3	6	138	703	357
$T_4 - S_3$	0	1	4	2	12	24	410
$T_1 - S_4$	0	0	0	6	16	124	25
$T_2 - S_4$	0	0	0	1	49	222	3
$T_3 - S_4$	0	51	232	1	1	17	91
$T_4 - S_4$	5	81	420	4	87	455	75

In the classical PDT Jablonski diagram, PDT processes require the excitation of the PS to the singlet excited state manifold S_X, followed by internal conversions and efficient intersystem crossing to lowest-lying singlet and triplet state, finally reaching the lowest triplet state, T_1. The triplet state population of thionucleobases and analogue systems is close to unity and has been extensively measured in the literature.[90] Structurally related compounds such as 6-thioguanosine and azathioprine, for instance, show an elevated triplet quantum yield, typically around 0.8.[91–93] Subsequently, the T_1 state quenching mechanisms are dominated by two distinct classes of photoreactions, the so-called type I and type II[94]. In type I PDT, the triplet state transfers or accepts an electron directly to surrounding molecules in the target tissue, often generating reactive oxygen species (ROS) through the formation of the superoxide anion

$O_2^{\bullet-}$. On the other hand, type II PDT consists of the energy transfer between the excited PS and molecular oxygen in the triplet ground state, $^3O_2$, to produce the highly oxidant singlet dioxygen, $^1O_2$:

$$^3(PS^*) + {}^3O_2 \rightarrow PS + {}^1O_2$$
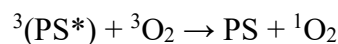
This type II mechanism is often dominant in PDT-active photosensitizers [95] and is thus studied here by comparing the energy levels of the triplet state of **6h** with the energy required to form $^1O_2$, measured[96] and computed[97] at 0.98 eV.[96,97] The vertical singlet–triplet energy gap ($\Delta E_{S\text{-}T}$) determined at the optimized T_1 geometry of **6h** is 1.52 eV (Figure 5), clearly larger than the energy level of $^1O_2$. Thus, the triplet state of the modified nucleoside **6h** possesses sufficient energy to photosensitize $^3O_2$. Singlet oxygen acts as a potent cytotoxic agent capable of inducing oxidative damage to cellular components, including lipids, proteins, and DNA, ideally causing apoptosis of the cancerous cell after irradiation. Note that the vertical T_2/T_1 energy difference (0.36 eV) shown in Figure 5 corresponds to the T_1 equilibrium geometry, consequently, it only applies when the system has already reached T_1.
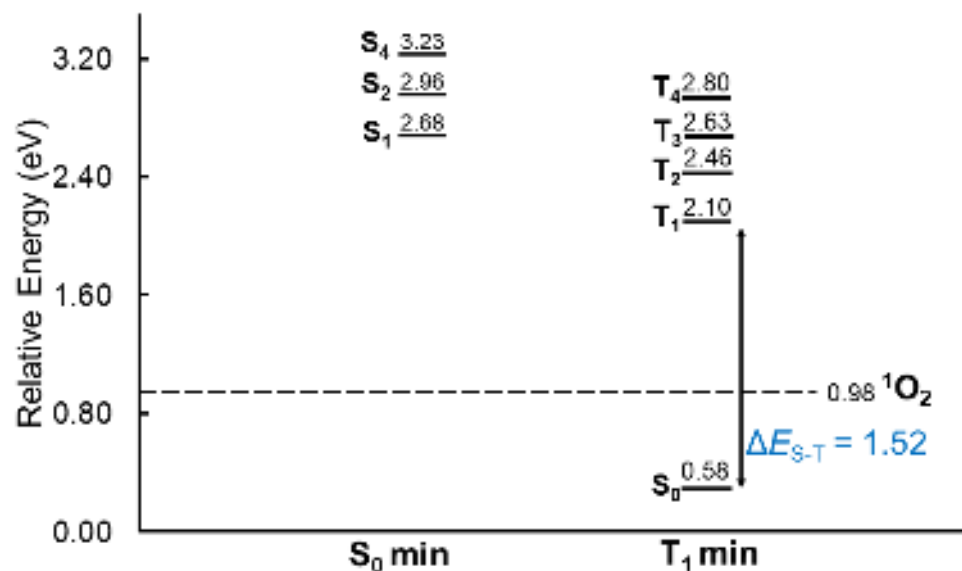

Figure 5. MS-CASPT2 vertical lowest singlet and triplet excitation energies (eV) for structure **6h** (solid lines) and O_2 (dashed lines). S_0 min and T_1 min geometries optimized with the DFT/B3LYP and TD-B3LYP methods, respectively.

IV. CONCLUSIONS AND PERSPECTIVES

This work describes the electronic absorption properties of a series of modified nucleobases and nucleosides with the aim to shift the typical UVB/UVA absorption of the chemotherapeutic agent gemcitabine to more biocompatible wavelengths in the visible region. This is achieved by combining a variety of chemical substitutions at the carbonylic oxygen (position 2, X = O, S, and Se), N1 (R_1), C5 (R_2), and N7 (R_3) positions of the pyrimidine core. The fluorine-containing sugar **DFS** at N1 aims to maintain the chemotherapeutic activity of gemcitabine in the dark based on the inhibition of the DNA polymerase, also in the designed photosensitizer. The π-conjugation is extended by linking an aromatic system to the C5 position (**VNT**, **TFS**, or **TTFS**), which dramatically red shifts the absorption energies, whereas substitution at N7 with squalene **SQ**, an intermediate in the cholesterol biosynthesis, ensures self-assembly properties to form micelles and slow down the rapid metabolism of gemcitabine in clinical conditions.

This work systematically appraises in detail the impact of the different substitution patterns on the absorption properties of the pyrimidine derivatives. The replacement of the carbonylic oxygen by the much heavier Se atom and the incorporation of the aromatic rings at the C5 position produce the largest red shifts. The 2-selenocytidine derivative with **TTFS** at the C5 position and the acetyl substitution at the N7 site (compound **6h**) shows the lowest energy absorption, fully covering yellow and orange wavelengths and partially reaching the red region in the vacuum. Analysis is based on accurate CASSCF/MS-CASPT2 computations employing large active spaces, while the optical spectra are simulated in water solution through a combination of classical molecular dynamics, QM/MM simulations and multiconfigurational MS-CASPT2/MM methods. Overall, the absorption properties of **6h** are satisfactory to serve as a prototype for PDT applications and represent a rational strategy to extend the optical properties of pyrimidines to the visible region upon chemical modifications based on biochemical criteria and synthetic evidence. The species **6d** and **6f** can be considered equally attractive although their optical properties have not been studied in the present work.

In spite of the absorption red shift and the large triplet state population induced by Se, the introduction of this heavy atom may also decrease the triplet lifetime of the chromophore, as recently observed by Crespo-Hernández and coworkers[90] and rationalized by González and collaborators[98] for 6-selenoguanine. The excited states of Te-substituted nucleobases are less explored although there is evidence of short triplet lifetimes as well.[99] Thus, the balance between red-shifting the absorption properties and enhancing the intersystem crossing capabilities is subtle, therefore, the possibility to resort on the S-substituted analogue of **6h** (or **6d/6f**) should be considered as well. As a matter of fact, results shown in Figure 1 for the candidates **5c** and **5d** also show strong red-shifted absorptions.

The use modified nucleobases with sulfur[100,101] or selenium,[88,102] or even with bulkier substituents at C5 position such as nitroimidazole derivatives[103,104] is well-known by the scientific community. Moreover, the possibility to combine PDT with other chemotherapeutical modes of action is an active research direction to improve photoinduced anticancer therapies and reduce its dependance on $^3O_2$. Some examples have been already reported in the literature, for instance by combining a photoactive transition metal complex with a *cis*-Pt like fragment,[97,105–107] or by administering a photosensitizer that generates radicals

and releases nitrogen mustards under light exposure.[34,108] There are conceptual differences between the cited examples and the possible dual action explored in this work. Here, the chemotherapeutic effect is not triggered by light, whereas in the Ru-Pt conjugates, firstly described by Brewer *et al.,* [106,109–111] light exposure indeed activates DNA alkylation. Therefore, the present approach should be considered as a possible chemotherapy/PDT dual action, whereas in other combined approaches labelled as PDT/photochemotherapy (PDT/PCT)[112,113] both modes of action are light-triggered.

Nonetheless, it is important to note that our conclusions only concern the optical properties of the studied molecules since, to the best of our knowledge, no biological data or anticancer activity in model experiments of the Se-containing candidates studied in this work is available in the literature. The chemotherapeutic mechanism of gemcitabine requires transport into the cell medium through the hENT1 carrier, followed by three phosphorylation steps exerted by a variety of kinases and by the DNA incorporation through the DNA polymerase.[14] At this stage it is unclear if the modifications proposed here will hold the biological activity of the original gemcitabine, however, previous studies with **SQ**-gemcitabine modifications have shown excellent anticancer activities.[16,17,83] Therefore, even though the approach is promising and the results on the optical properties are solid, caution should be taken when interpreting the results presented in this work since no biological activity information can be inferred from the present analyses.

SUPPLEMENTARY MATERIAL

Additional analyses on the CAS active spaces, study of the number of SA-CASSCF roots, basis set size, and relativistic effects on the vertical absorption energies.

ACKNOWLEDGEMENTS

AUTHOR DECLARATIONS

Conflict of Interest

The authors have no conflicts to disclose.

DATA AVAILABILITY

The data that supports the findings of this study can be reproduced with the details given in the article and in the supplementary information. The quantum chemistry programs OpenMolcas and ORCA 5 are license-free and publicly available. The Gaussian 16 software is publicly available. All data reported here is available from the corresponding author upon request.

REFERENCES

[1] P. Singh, M. Yam, P.J. Russell, and A. Khatri, "Molecular and traditional chemotherapy: A united front against prostate cancer," Cancer Lett **293**(1), 1–14 (2010).

[2] V.T. DeVita Jr., and E. Chu, "A History of Cancer Chemotherapy," Cancer Res **68**(21), 8643–8653 (2008).

[3] Z.H. Siddik, "Cisplatin: mode of cytotoxic action and molecular basis of resistance," Oncogene **22**(47), 7265–7279 (2003).

[4] E. De Clercq, "Antivirals: Past, present and future," Biochem Pharmacol **85**(6), 727–744 (2013).

[5] Q. Zeng, H. Zhang, P. Kuang, J. Li, X. Chen, T. Dong, Q. Wu, C. Zhang, C. Chen, T. Niu, T. Liu, Z. Liu, and J. Ji, "A novel conditioning regimen of chidamide, cladribine, gemcitabine, and busulfan in the autologous stem cell transplantation of aggressive T-cell lymphoma," Front Oncol **13**, (2023).

[6] C.M. Galmarini, J.R. Mackey, and C. Dumontet, "Nucleoside analogues and nucleobases in cancer treatment," Lancet Oncol **3**(7), 415–424 (2002).

[7] V. Schirrmacher, "From chemotherapy to biological therapy: A review of novel concepts to reduce the side effects of systemic cancer treatment (Review)," Int J Oncol **54**(2), 407–419 (2019).

[8] S. Monro, K.L. Colón, H. Yin, J.I.I.I. Roque, P. Konda, S. Gujar, R.P. Thummel, L. Lilge, C.G. Cameron, and S.A. McFarland, "Transition Metal Complexes and Photodynamic Therapy from a Tumor-Centered Approach: Challenges, Opportunities, and Highlights from the Development of TLD1433," Chem Rev **119**(2), 797–828 (2019).

[9] R. Improta, and T. Douki, *DNA Photodamage: From Light Absorption to Cellular Responses and Skin Cancer* (The Royal Society of Chemistry, 2021).

[10] T. Yano, and K.K. Wang, "Photodynamic Therapy for Gastrointestinal Cancer," Photochem Photobiol **96**(3), 517–523 (2020).

[11] S. Zeng, M. Pöttler, B. Lan, R. Grützmann, C. Pilarsky, and H. Yang, "Chemoresistance in pancreatic cancer," Int J Mol Sci **20**(18), (2019).

[12] L. Toschi, G. Finocchiaro, S. Bartolini, V. Gioia, and & F. Cappuzzo, "Drug Evaluation Role of gemcitabine in cancer therapy," Future Oncology **1**(1), 7–17 (2005).

[13] E. Mini, S. Nobili, B. Caciagli, I. Landini, and T. Mazzei, "Cellular pharmacology of gemcitabine," Annals of Oncology **17**(SUPPL. 5), (2006).

[14] E. Artin, J. Wang, G.J.S. Lohman, K. Yokoyama, G. Yu, R.G. Griffin, G. Bar, and J.A. Stubbe, "Insight into the mechanism of inactivation of ribonucleotide reductase by gemcitabine 5′-diphosphate in the presence or absence of reductant," Biochemistry **48**(49), 11622–11629 (2009).

[15] E. Moysan, G. Bastiat, and J.P. Benoit, "Gemcitabine versus modified gemcitabine: A review of several promising chemical modifications," Mol Pharm **10**(2), 430–444 (2013).

[16] P. Couvreur, L.H. Reddy, S. Mangenot, J.H. Poupaert, D. Desmaële, S. Lepêtre-Mouelhi, B. Pili, C. Bourgaux, H. Amenitsch, and M. Ollivon, "Discovery of New Hexagonal Supramolecular Nanostructures Formed by Squalenoylation of an Anticancer Nucleoside Analogue," Small **4**(2), 247–253 (2008).

[17] L.H. Reddy, C. Dubernet, S.L. Mouelhi, P.E. Marque, D. Desmaele, and P. Couvreur, "A new nanomedicine of gemcitabine displays enhanced anticancer activity in sensitive and resistant leukemia types," J Control Release **124**(1–2), 20–27 (2007).

[18] L. Martínez-Fernández, and A. Francés-Monerris, in *Theoretical and Computational Photochemistry*, edited by C. García-Iriepa and M. Marazzi (Elsevier, 2023), pp. 311–336.

[19] R. Improta, F. Santoro, and L. Blancafort, "Quantum Mechanical Studies on the Photophysics and the Photochemistry of Nucleic Acids and Nucleobases," Chem Rev **116**(6), 3540–3593 (2016).

[20] A. Francés-Monerris, H. Gattuso, D. Roca-Sanjuán, I. Tuñón, M. Marazzi, E. Dumont, and A. Monari, "Dynamics of the excited-state hydrogen transfer in a (dG)·(dC) homopolymer: Intrinsic photostability of DNA," Chem Sci **9**(41), 7902–7911 (2018).

[21] A.A. Beckstead, Y. Zhang, M.S. de Vries, and B. Kohler, "Life in the light: nucleic acid photoproperties as a legacy of chemical evolution," Phys Chem Chem Phys **18**(35), 24228–24238 (2016).

[22] M. Merchán, R. González-Luque, T. Climent, L. Serrano-Andrés, E. Rodríguez, M. Reguero, and D. Peláez, "Unified model for the ultrafast decay of pyrimidine nucleobases," J Phys Chem B **110**(51), 26471–26476 (2006).

[23] R. Improta, F. Santoro, and L. Blancafort, "Quantum Mechanical Studies on the Photophysics and the Photochemistry of Nucleic Acids and Nucleobases," Chem Rev **116**(6), 3540–3593 (2016).

[24] L. Martínez Fernández, F. Santoro, and R. Improta, "Nucleic Acids as a Playground for the Computational Study of the Photophysics and Photochemistry of Multichromophore Assemblies," Acc Chem Res **55**(15), 2077–2087 (2022).

[25] J.T. Reardon, and A. Sancar, in Prog Nucleic Acid Res Mol Biol (Academic Press, 2005), pp. 183–235.

[26] C.E. Crespo-Hernández, B. Cohen, P.M. Hare, and B. Kohler, "Ultrafast excited-state dynamics in nucleic acids," Chem Rev **104**(4), 1977–2019 (2004).

[27] K. Zhang, F. Wang, Y. Jiang, X. Wang, H. Pan, Z. Sun, H. Sun, J. Xu, and J. Chen, "New Insights about the Photostability of DNA/RNA Bases: Triplet nπ∗ State Leads to Effective Intersystem Crossing in Pyrimidinones," J Phys Chem B **125**(8), 2042–2049 (2021).

[28] S. Zhou, H. Tian, J. Yan, Z. Zhang, G. Wang, X. Yu, W. Sang, B. Li, G.S.P. Mok, J. Song, and Y. Dai, "IR780/Gemcitabine-conjugated metal-phenolic network enhanced photodynamic cancer therapy," Chinese Chem Lett, 108312 (2023).

[29] R.R. Allison, and K. Moghissi, "Photodynamic therapy (PDT): PDT mechanisms," Clin Endosc **46**(1), 24 (2013).

[30] K. Andersson, P. Malmqvist, and B.O. Roos, "Second-order perturbation theory with a complete active space self-consistent field reference function," J Chem Phys **96**(2), 1218–1226 (1992).

[31] D. Roca-Sanjuán, F. Aquilante, and R. Lindh, "Multiconfiguration second-order perturbation theory approach to strong electron correlation in chemistry and photochemistry," WIREs Comp Mol Sci **2**(4), 585–603 (2012).

[32] H. Lischka, D. Nachtigallová, A.J.A. Aquino, P.G. Szalay, F. Plasser, F.B.C. Machado, and M. Barbatti, "Multireference Approaches for Excited States of Molecules," Chem Rev **118**(15), 7293–7361 (2018).

[33] J. Finley, A. Malmqvist, B.O. Roos, L. Serrano-Andres¨´, and A. Andres, "The Multi-State CASPT2 Method", Chem Phys Lett **288**(2-4), 299-306 (1998).

[34] A.M.A. Abdelgawwad, A. Monari, I. Tuñón, and A. Francés-Monerris, "Spatial and Temporal Resolution of the Oxygen-Independent Photoinduced DNA Interstrand Cross-Linking by a Nitroimidazole Derivative," J Chem Inf Model **62**(13), 3239–3252 (2022).

[35] L.-Y. Peng, Z.-W. Li, Q. Fang, B.-B. Xie, S.-H. Xia, and G. Cui, "Combined QM (MS-CASPT2)/MM studies on photocyclization and photoisomerization of a fulgide derivative in toluene solution," Phys Chem Chem Phys **24**(48), 29918–29926 (2022).

[36] A. Frances-Monerris, J. Segarra-Marti, M. Merchan, and D. Roca-Sanjuan, "Complete-active-space second-order perturbation theory (CASPT2//CASSCF) study of the dissociative electron attachment in canonical DNA nucleobases caused by low-energy electrons (0-3 eV)," J Chem Phys **143**(21), 215101 (2015).

[37] A. Francés-Monerris, M. Merchán, and D. Roca-Sanjuán, "Communication: Electronic UV-Vis transient spectra of the ·oH reaction products of uracil, thymine, cytosine, and 5,6-dihydrouracil by using the complete active space self-consistent field second-order perturbation (CASPT2//CASSCF) theory," J Chem Phys **139**(7), (2013).

[38] S. Mai, B. Ashwood, P. Marquetand, C.E. Crespo-Hernández, and L. González, "Solvatochromic Effects on the Absorption Spectrum of 2-Thiocytosine," J Phys Chem B **121**(20), 5187–5196 (2017).

[39] A. Francés-Monerris, C. Hognon, M.A. Miranda, V. Lhiaubet-Vallet, and A. Monari, "Triplet photosensitization mechanism of thymine by an oxidized nucleobase: From a dimeric model to DNA environment," Phys Chem Chem Phys **20**(40), 25666–25675 (2018).

[40] L. Serrano-Andrés, and M. Merchán, "Are the five natural DNA/RNA base monomers a good choice from natural selection?. A photochemical perspective," Journal of Photochemistry and Photobiology C: Photochemistry Reviews **10**(1), 21–32 (2009).

[41] D. Roca-Sanjuán, G. Olaso-González, M. Rubio, P.B. Coto, M. Merchán, N. Ferré, V. Ludwig, and L. Serrano-Andrés, in *Pure and Applied Chemistry* (2009), pp. 743–754.

[42] R. Krishnan, J.S. Binkley, R. Seeger, and J.A. Pople, "Self-consistent molecular orbital methods. XX. A basis set for correlated wave functions," J Chem Phys **72**(1), 650–654 (1980).

[43] M.J. Frisch, G.W. Trucks, H.B. Schlegel, G.E. Scuseria, M. a. Robb, J.R. Cheeseman, G. Scalmani, V. Barone, G. a. Petersson, H. Nakatsuji, X. Li, M. Caricato, a. V. Marenich, J. Bloino, B.G. Janesko, R. Gomperts, B. Mennucci, H.P. Hratchian, J. V. Ortiz, a. F. Izmaylov, J.L. Sonnenberg, Williams, F. Ding, F. Lipparini, F. Egidi, J. Goings, B. Peng, A. Petrone, T. Henderson, D. Ranasinghe, V.G. Zakrzewski, J. Gao, N. Rega, G. Zheng, W. Liang, M. Hada, M. Ehara, K. Toyota, R. Fukuda, J. Hasegawa, M. Ishida, T. Nakajima, Y. Honda, O. Kitao, H. Nakai, T. Vreven, K. Throssell, J. a. Montgomery Jr., J.E. Peralta, F. Ogliaro, M.J. Bearpark, J.J. Heyd, E.N. Brothers, K.N. Kudin, V.N. Staroverov, T. a. Keith, R. Kobayashi, J. Normand, K. Raghavachari, a. P. Rendell, J.C. Burant, S.S. Iyengar, J. Tomasi, M. Cossi, J.M. Millam, M. Klene, C. Adamo, R. Cammi, J.W. Ochterski, R.L. Martin, K. Morokuma, O. Farkas, J.B. Foresman, and D.J. Fox, "G16_C01," Gaussian 16, Revision C.01, Gaussian, Inc., Wallington (2016).

[44] C. Butchosa, S. Simon, and A.A. Voityuk, "Electron transfer from aromatic amino acids to guanine and adenine radical cations in π stacked and T-shaped complexes," Org Biomol Chem **8**(8), 1870–1875 (2010).

[45] S. Bai, and M. Barbatti, "On the decay of the triplet state of thionucleobases," Phys Chem Chem Phys **19**(20), 12674–12682 (2017).

[46] S. Eynollahi, S. Riahi, M.R. Ganjali, and P. Norouzi, "Density functional theory studies on the geometry and electronic properties of Mitomycin C, DNA Base Pairs and their complex," Int J Electrochem Sci **5**(9), 1367–1378 (2010).

[47] K. Andersson, P.Å. Malmqvist, B.O. Roos, A.J. Sadlej, and K. Wolinski, "Second-order perturbation theory with a CASSCF reference function," J Phys Chem **94**(14), 5483–5488 (1990).

[48] P.-Å. Malmqvist, and B.O. Roos, "The CASSCF state interaction method," Chem Phys Lett **155**(2), 189–194 (1989).

[49] B.O. Roos, V. Veryazov, and P.-O. Widmark, "Relativistic atomic natural orbital type basis sets for the alkaline and alkaline-earth atoms applied to the ground-state potentials for the corresponding dimers," Theor Chem Acc **111**(2), 345–351 (2004).

[50] P. Kimber, and F. Plasser, "Toward an understanding of electronic excitation energies beyond the molecular orbital picture," Phys Chem Chem Phys **22**(11), 6058–6080 (2020).

[51] G. Ghigo, B.O. Roos, and P.-Å. Malmqvist, "A modified definition of the zeroth-order Hamiltonian in multiconfigurational perturbation theory (CASPT2)," Chem Phys Lett **396**(1), 142–149 (2004).

[52] Q. Peng, Y.H. Zhu, T.S. Zhang, X.Y. Liu, W.H. Fang, and G. Cui, "Selenium substitution effects on excited-state properties and photophysics of uracil: a MS-CASPT2 study," Phys Chem Chem Phys **22**(21), 12120–12128 (2020).

[53] B.O. Roos, R. Lindh, P.-Å. Malmqvist, V. Veryazov, and P.-O. Widmark, "New Relativistic ANO Basis Sets for Transition Metal Atoms," J Phys Chem A **109**(29), 6575–6579 (2005).

[54] A.M.A. Abdelgawwad, J.A.M. Xavier, D. Roca-Sanjuán, C. Viñas, F. Teixidor, and A. Francés-Monerris, "Light-Induced On/Off Switching of the Surfactant Character of the o-Cobaltabis(dicarbollide) Anion with No Covalent Bond Alteration," Angew. Chem. In. Ed. **60**(49), 25753–25757 (2021).

[55] P.Å. Malmqvist, B.O. Roos, and B. Schimmelpfennig, "The restricted active space (RAS) state interaction approach with spin–orbit coupling," Chem Phys Lett **357**(3), 230–240 (2002).

[56] P.-Å. Malmqvist, and B.O. Roos, "The CASSCF state interaction method," Chem Phys Lett **155**(2), 189–194 (1989).

[57] I. Fernández Galván, M. Vacher, A. Alavi, C. Angeli, F. Aquilante, J. Autschbach, J.J. Bao, S.I. Bokarev, N.A. Bogdanov, R.K. Carlson, L.F. Chibotaru, J. Creutzberg, N. Dattani, M.G. Delcey, S.S. Dong, A. Dreuw, L. Freitag, L.M. Frutos, L. Gagliardi, F. Gendron, A.

Giussani, L. Gonzalez, G. Grell, M. Guo, C.E. Hoyer, M. Johansson, S. Keller, S. Knecht, G. Kovačević, E. Källman, G. Li Manni, M. Lundberg, Y. Ma, S. Mai, J.P. Malhado, P.A. Malmqvist, P. Marquetand, S.A. Mewes, J. Norell, M. Olivucci, M. Oppel, Q.M. Phung, K. Pierloot, F. Plasser, M. Reiher, A.M. Sand, I. Schapiro, P. Sharma, C.J. Stein, L.K. Sørensen, D.G. Truhlar, M. Ugandi, L. Ungur, A. Valentini, S. Vancoillie, V. Veryazov, O. Weser, T.A. Wesolowski, P.-O. Widmark, S. Wouters, A. Zech, J.P. Zobel, and R. Lindh, "OpenMolcas: From source code to insight," J Chem Theory Comput **15**(11), 5925–5964 (2019).

[58] D.A. Case, H.M. Aktulga, K. Belfon, I.Y. Ben-Shalom, S.R. Brozell, D.S. Cerutti, T.E. Cheatham III, G.A. Cisneros, V.W.D. Cruzeiro, T.A. Darden, R.E. Duke, G. Giambasu, M.K. Gilson, H. Gohlke, A.W. Goetz, R. Harris, S. Izadi, S.A. Izmailov, C. Jin, K. Kasavajhala, M.C. Kaymak, E. King, A. Kovalenko, T. Kurtzman, T.S. Lee, S. LeGrand, P. Li, C. Lin, J. Liu, T. Luchko, R. Luo, M. Machado, V. Man, M. Manathunga, K.M. Merz, Y. Miao, O. Mikhailovskii, G. Monard, H. Nguyen, K.A. O'Hearn, A. Onufriev, F. Pan, S. Pantano, R. Qi, A. Rahnamoun, D.R. Roe, A. Roitberg, C. Sagui, S. Schott-Verdugo, J. Shen, C.L. Simmerling, N.R. Skrynnikov, J. Smith, J. Swails, R.C. Walker, J. Wang, H. Wei, R.M. Wolf, X. Wu, Y. Xue, D.M. York, S. Zhao, and P.A. Kollman, "Amber 20," Amber 20, San Francisco (2021).

[59] A. Pérez, I. Marchán, D. Svozil, J. Sponer, T.E. Cheatham, C.A. Laughton, and M. Orozco, "Refinement of the AMBER Force Field for Nucleic Acids: Improving the Description of α/γ Conformers," Biophys J **92**(11), 3817–3829 (2007).

[60] W.D. Cornell, P. Cieplak, C.I. Bayly, and P.A. Kollman, "Application of RESP charges," Journal of American Chemical Society **115**(7), 9620–9631 (1993).

[61] W.L. Jorgensen, J. Chandrasekhar, J.D. Madura, R.W. Impey, and M.L. Klein, "Comparison of simple potential functions for simulating liquid water," J Chem Phys **79**(2), 926–935 (1983).

[62] S. Sitkiewicz, J. Carmona-García, L. Cerdán, and D. Roca-Sanjuán, "MULTISPEC," (2023). https://github.com/qcexval/multispec (accesed on October 20th)

[63] F. Neese, F. Wennmohs, U. Becker, and C. Riplinger, "The ORCA quantum chemistry program package," J Chem Phys **152**(22), 224108 (2020).

[64] M. Barbatti, M. Ruckenbauer, F. Plasser, J. Pittner, G. Granucci, M. Persico, and H. Lischka, "Newton-X: A surface-hopping program for nonadiabatic molecular dynamics," WIREs Comput Mol Sci **4**(1), 26–33 (2014).

[65] M. Barbatti, M. Bondanza, R. Crespo-Otero, B. Demoulin, P.O. Dral, G. Granucci, F. Kossoski, H. Lischka, B. Mennucci, S. Mukherjee, M. Pederzoli, M. Persico, M. Pinheiro Jr, J. Pittner, F. Plasser, E. Sangiogo Gil, and L. Stojanovic, "Newton-X Platform: New Software Developments for Surface Hopping and Nuclear Ensembles," J Chem Theory Comput **18**(11), 6851–6865 (2022).

[66] E. van Lenthe, E.J. Baerends, and J.G. Snijders, "Relativistic regular two-component Hamiltonians," J Chem Phys **99**(6), 4597–4610 (1993).

[67] M. Merchán, L. Serrano-Andrés, M.A. Robb, and L. Blancafort, "Triplet-state formation along the ultrafast decay of excited singlet cytosine," J Am Chem Soc **127**(6), 1820–1825 (2005).

[68] B.H. Ng, and J.W. Anderson, "Synthesis of selenocysteine by cysteine synthases from selenium accumulator and non-accumulator plants," Phytochemistry **17**(12), 2069–2074 (1978).

[69] K.F. Hellendahl, F. Kaspar, X. Zhou, Z. Yang, Z. Huang, P. Neubauer, and A. Kurreck, "Optimized Biocatalytic Synthesis of 2-Selenopyrimidine Nucleosides by Transglycosylation**," ChemBioChem **22**(11), 2002–2009 (2021).

[70] R. Shapiro, "Prebiotic cytosine synthesis: A critical analysis and implications for the origin of life," Proc Natl Acad Sci USA **96**(8), 4396–4401 (1999).

[71] H. Zhen, J. Sharon, Y. Zhaoyi, and L.I.U. Daxue, Patent: "Synthesis method of nucleoside compound," (2017). China National Intellectual Property Administration

[72] E.S. Scherbinina, D. V Dar'in, and P.S. Lobanov, "Investigation on possibility of rearrangement of pyrimidine-5-carboxylic acids esters," Chem Heterocycl Compd (N Y) **46**(9), 1109–1115 (2010).

[73] H. Zhen, J. Sharon, Y. Zhaoyi, and L.I.U. Daxue, Patent: "Novel nucleoside compounds and preparation method thereof," (2017). China National Intellectual Property Administration

[74] K. Brown, M. Dixey, A. Weymouth-Wilson, and B. Linclau, "The synthesis of gemcitabine," Carbohydr Res **387**(1), 59–73 (2014).

[75] S. Ogasawara, and M. Maeda, "Photochromic nucleobase: reversible photoisomerization, photochemical properties and photoregulation of hybridization.," Nucleic Acids Symp Ser (Oxf) (52), 369–370 (2008).

[76] M. Kovaliov, M. Segal, and B. Fischer, "Fluorescent p-substituted-phenyl-imidazolo-cytidine analogues," Tetrahedron **69**(18), 3698–3705 (2013).

[77] M. Segal, and B. Fischer, "Analogues of uracil nucleosides with intrinsic fluorescence (NIF-analogues): Synthesis and photophysical properties," Org Biomol Chem **10**(8), 1571–1580 (2012).

[78] M. Alauddin, and M. Abdul Aziz, "Spectroscopic properties of cytosine: a computational investigation," Barisal University Journal Part 1 **4**(2), 227–235 (2017).

[79] S. Mai, M. Pollum, L. Martínez-Fernández, N. Dunn, P. Marquetand, I. Corral, C.E. Crespo-Hernández, and L. González, "The origin of efficient triplet state population in sulfur-substituted nucleobases," Nat Commun **7**, (2016).

[80] N. Mahar, V. Vetrivelan, S. Muthu, S. Javed, and A.A. Al-Saadi, "Surface enhanced Raman spectra (SERS) and computational study of gemcitabine drug adsorption on to Au/Ag clusters with different complexes: Adsorption behavior and solvent effect (IEFPCM) – Anticancer agent," Comput Theor Chem **1217**, (2022).

[81] T. Kaur, S. Kaur, and P. Kaur, "Development and validation of UV-spectrophotometric methods for determination of gemcitabine hydrochloride in bulk and polymeric nanoparticles," Int J Appl Pharmaceut **9**(5), 60–65 (2017).

[82] M.S. Ali, M. Waseem, N. Subbarao, and H.A. Al-Lohedan, "Noncovalent molecular interactions between antineoplastic drug gemcitabine and a carrier protein identified through spectroscopic and in silico methods," Int J Biol Macromol **182**, 993–1002 (2021).

[83] D. Desmaële, R. Gref, and P. Couvreur, "Squalenoylation: A generic platform for nanoparticular drug delivery," J Control Release **161**(2), 609–618 (2012).

[84] A. Francés-Monerris, M. Lineros-Rosa, M.A.A. Miranda, V. Lhiaubet-Vallet, and A. Monari, "Photoinduced Intersystem Crossing in DNA Oxidative Lesions and Epigenetic Intermediates," Chem Commun **56**, 4404–4407 (2020).

[85] M. Lineros-Rosa, A. Francés-Monerris, A. Monari, M.A. Miranda, and V. Lhiaubet-Vallet, "Experimental and theoretical studies on thymine photodimerization mediated by oxidatively generated DNA lesions and epigenetic intermediates," Phys Chem Chem Phys **22**, 25661–25668 (2020).

[86] T.F.J. Kraus, D. Globisch, M. Wagner, S. Eigenbrod, D. Widmann, M. Münzel, M. Müller, T. Pfaffeneder, B. Hackner, W. Feiden, U. Schüller, T. Carell, and H.A. Kretzschmar, "Low values of 5-hydroxymethylcytosine (5hmC), the 'sixth base,' are associated with anaplasia in human brain tumors," Int J Cancer **131**(7), 1577–1590 (2012).

[87] C.M. Marian, "Spin-orbit coupling and intersystem crossing in molecules," WIREs Comput Mol Sci **2**(2), 187–203 (2012).

[88] Y.G. Fang, D. Valverde, S. Mai, S. Canuto, A.C. Borin, G. Cui, and L. Gonzaìlez, "Excited-state properties and relaxation pathways of selenium-substituted guanine nucleobase in aqueous solution and DNA duplex," J Phys Chem B **125**(7), 1778–1789 (2021).

[89] Q. Peng, Y.H. Zhu, T.S. Zhang, X.Y. Liu, W.H. Fang, and G. Cui, "Selenium substitution effects on excited-state properties and photophysics of uracil: a MS-CASPT2 study," Phys Chem Chem Phys **22**(21), 12120–12128 (2020).

[90] K.M. Farrell, M.M. Brister, M. Pittelkow, T.I. Sølling, and C.E. Crespo-Hernández, "Heavy-Atom-Substituted Nucleobases in Photodynamic Applications: Substitution of Sulfur with Selenium in 6-Thioguanine Induces a Remarkable Increase in the Rate of Triplet Decay in 6-Selenoguanine," J Am Chem Soc **140**(36), 11214–11218 (2018).

[91] C. Reichardt, C. Guo, and C.E. Crespo-Hernández, "Excited-State Dynamics in 6-Thioguanosine from the Femtosecond to Microsecond Time Scale," J Phys Chem B **115**(12), 3263–3270 (2011).

[92] B. Ashwood, M. Pollum, and C.E. Crespo-Hernández, "Photochemical and Photodynamical Properties of Sulfur-Substituted Nucleic Acid Bases," Photochem Photobiol **95**(1), 33–58 (2019).

93 L.A. Ortiz-Rodríguez, G. Ortiz-Zayas, M. Pollum, S.J. Hoehn, S. Jockusch, and C.E. Crespo-Hernández, "Intramolecular Charge Transfer in the Azathioprine Prodrug Quenches Intersystem Crossing to the Reactive Triplet State in 6-Mercaptopurine†," Photochem Photobiol **98**(3), 617–632 (2022).

94 S. Yano, S. Hirohara, M. Obata, Y. Hagiya, S. ichiro Ogura, A. Ikeda, H. Kataoka, M. Tanaka, and T. Joh, "Current states and future views in photodynamic therapy," Journal of Photochemistry and Photobiology C: Photochemistry Reviews **12**(1), 46–67 (2011).

95 T. Yano, and K.K. Wang, "Photodynamic Therapy for Gastrointestinal Cancer," Photochem Photobiol **96**(3), 517–523 (2020).

96 M.E. Alberto, J. Pirillo, N. Russo, and C. Adamo, "Theoretical Exploration of Type I/Type II Dual Photoreactivity of Promising Ru(II) Dyads for PDT Approach," Inorg Chem **55**(21), 11185–11192 (2016).

97 M.E. Alberto, N. Russo, and A. Carlo, "Synergistic Effects of Metals in a Promising Ru(II)−Pt(II) Assembly for a Combined Anticancer Approach: Theoretical Exploration of the Photophysical Properties," Chem Eur J **22**(27), 9162–9168 (2016).

98 D. Valverde, S. Mai, S. Canuto, A.C. Borin, and L. González, "Ultrafast Intersystem Crossing Dynamics of 6-Selenoguanine in Water," JACS Au **2**(7), 1699–1711 (2022).

99 X.-P. Chang, J.-L. Wang, L.-Y. Peng, X.-J. Cen, B.-W. Yin, and B.-B. Xie, "Mechanistic photophysics of tellurium-substituted cytosine: Electronic structure calculations and nonadiabatic dynamics simulations1," Photochem Photobiol **00**(n/a), 1–16 (2023).

100 S. Mai, M. Pollum, L. Martínez-Fernández, N. Dunn, P. Marquetand, I. Corral, C.E. Crespo-Hernández, and L. González, "The origin of efficient triplet state population in sulfur-substituted nucleobases," Nat Commun **7**(1), 13077 (2016).

101 L. Martínez-Fernández, I. Corral, G. Granucci, and M. Persico, "Competing ultrafast intersystem crossing and internal conversion: A time resolved picture for the deactivation of 6-thioguanine," Chem Sci **5**(4), 1336–1347 (2014).

102 X. Peng, S.H. In, H. Li, M.M. Seidman, and M.M. Greenberg, "Interstrand cross-link formation in duplex and triplex DNA by modified pyrimidines," J Am Chem Soc **130**(31), 10299–10306 (2008).

103 A. Francés-Monerris, I. Tuñón, and A. Monari, "Hypoxia-Selective Dissociation Mechanism of a Nitroimidazole Nucleoside in a DNA Environment," J Phys Chem Lett **10**(21), 6750–6754 (2019).

104 Y. Kuang, H. Sun, J.C. Blain, and X. Peng, "Hypoxia-Selective DNA Interstrand Cross-Link Formation by Two Modified Nucleosides," Chem Eur J **18**(40), 12609–12613 (2012).

105 M.E. Alberto, and A. Francés-Monerris, "A multiscale free energy method reveals an unprecedented photoactivation of a bimetallic Os(ii)–Pt(ii) dual anticancer agent," Phys Chem Chem Phys **24**(32), 19584–19594 (2022).

106 S.L.H. Higgins, A.J. Tucker, B.S.J. Winkel, and K.J. Brewer, "Metal to ligand charge transfer induced DNA photobinding in a Ru(ii)–Pt(ii) supramolecule using red light in the therapeutic window: a new mechanism for DNA modification," Chem Commun **48**(1), 67–69 (2012).

107 S.L.H. Higgins, T.A. White, B.S.J. Winkel, and K.J. Brewer, "Redox, Spectroscopic, and Photophysical Properties of Ru−Pt Mixed-Metal Complexes Incorporating 4,7-Diphenyl-1,10-phenanthroline as Efficient DNA Binding and Photocleaving Agents," Inorg Chem **50**(2), 463–470 (2011).

108 Y. Han, W. Chen, Y. Kuang, H. Sun, Z. Wang, and X. Peng, "UV-Induced DNA Interstrand Cross-Linking and Direct Strand Breaks from a New Type of Binitroimidazole Analogue," Chem Res Toxicol **28**(5), 919–926 (2015).

109 R.L. Williams, H.N. Toft, B. Winkel, and K.J. Brewer, "Synthesis, Characterization, and DNA Binding Properties of a Series of Ru, Pt Mixed-Metal Complexes," Inorg Chem **42**(14), 4394–4400 (2003).

110 M. Milkevitch, H. Storrie, E. Brauns, K.J. Brewer, and B.W. Shirley, "A New Class of Supramolecular, Mixed-Metal DNA-Binding Agents: The Interaction of RuII,PtII and OsII,PtII Bimetallic Complexes with DNA," Inorg Chem **36**(20), 4534–4538 (1997).

111 S.L.H. Higgins, T.A. White, B.S.J. Winkel, and K.J. Brewer, "Redox, Spectroscopic, and Photophysical Properties of Ru−Pt Mixed-Metal Complexes Incorporating 4,7-Diphenyl-1,10-phenanthroline as Efficient DNA Binding and Photocleaving Agents," Inorg Chem **50**(2), 463–470 (2011).

[112] J.A. Roque III, H.D. Cole, P.C. Barrett, L.M. Lifshits, R.O. Hodges, S. Kim, G. Deep, A. Francés-Monerris, M.E. Alberto, C.G. Cameron, and S.A. McFarland, "Intraligand Excited States Turn a Ruthenium Oligothiophene Complex into a Light-Triggered Ubertoxin with Anticancer Effects in Extreme Hypoxia," J Am Chem Soc **144**(18), 8317–8336 (2022).

[113] H.D. Cole, J.A.I.I.I. Roque, G. Shi, L.M. Lifshits, E. Ramasamy, P.C. Barrett, R.O. Hodges, C.G. Cameron, and S.A. McFarland, "Anticancer Agent with Inexplicable Potency in Extreme Hypoxia: Characterizing a Light-Triggered Ruthenium Ubertoxin," J Am Chem Soc **144**(22), 9543–9547 (2022).